Electronic Supplementary Information

PH-controllable Regeneration and Visible-light Photocatalytic Redox of Carbon and Nitrogen Codoped $Zn_3Nb_2O_8$ towards Multiple Contaminants

Ping Bai, Niri Wu, Yuanjiang Wang, Ting Yang, Hui Li, Jingyu Zhang, Zhanli Chai*, Xiaojing Wang

Inner Mongolia Key Laboratory of Chemistry and Physics of Rare Earth Materials, School of Chemistry and Chemical Engineering, Inner Mongolia University, Inner Mongolia 010021, People's Republic of China

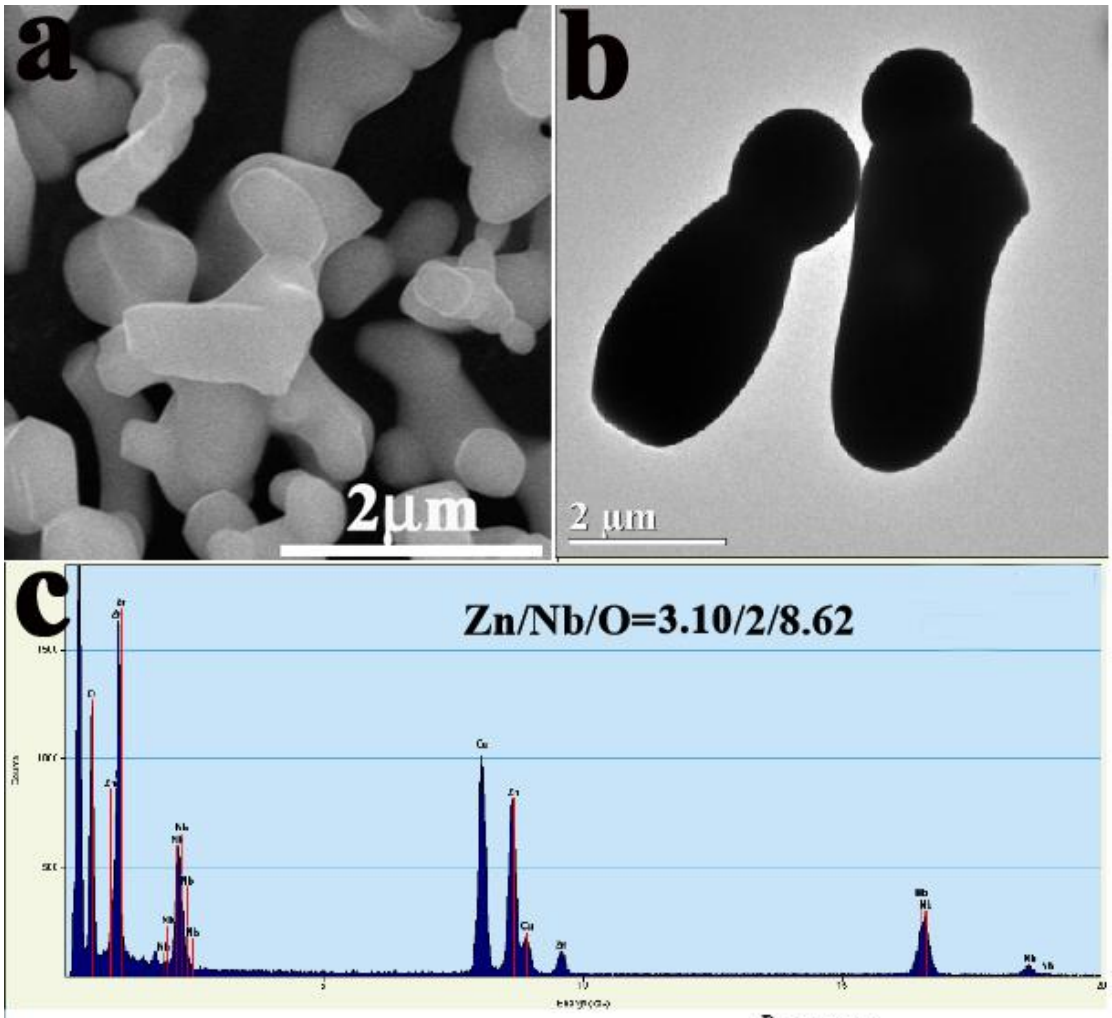

Element	Weight %	Atomic %	Uncert. %	Detector Correction	k-Factor
O(K)	26.18	62.80	0.29	0.51	1.889
Zn(K)	38.56	22.63	0.29	0.99	1.755
Nb(K)	35.25	14.56	0.44	0.99	4.007

Fig. S1. SEM image (a) and TEM image (b), and EDS analysis (c) of as-obtained pure $Zn_3Nb_2O_8$.

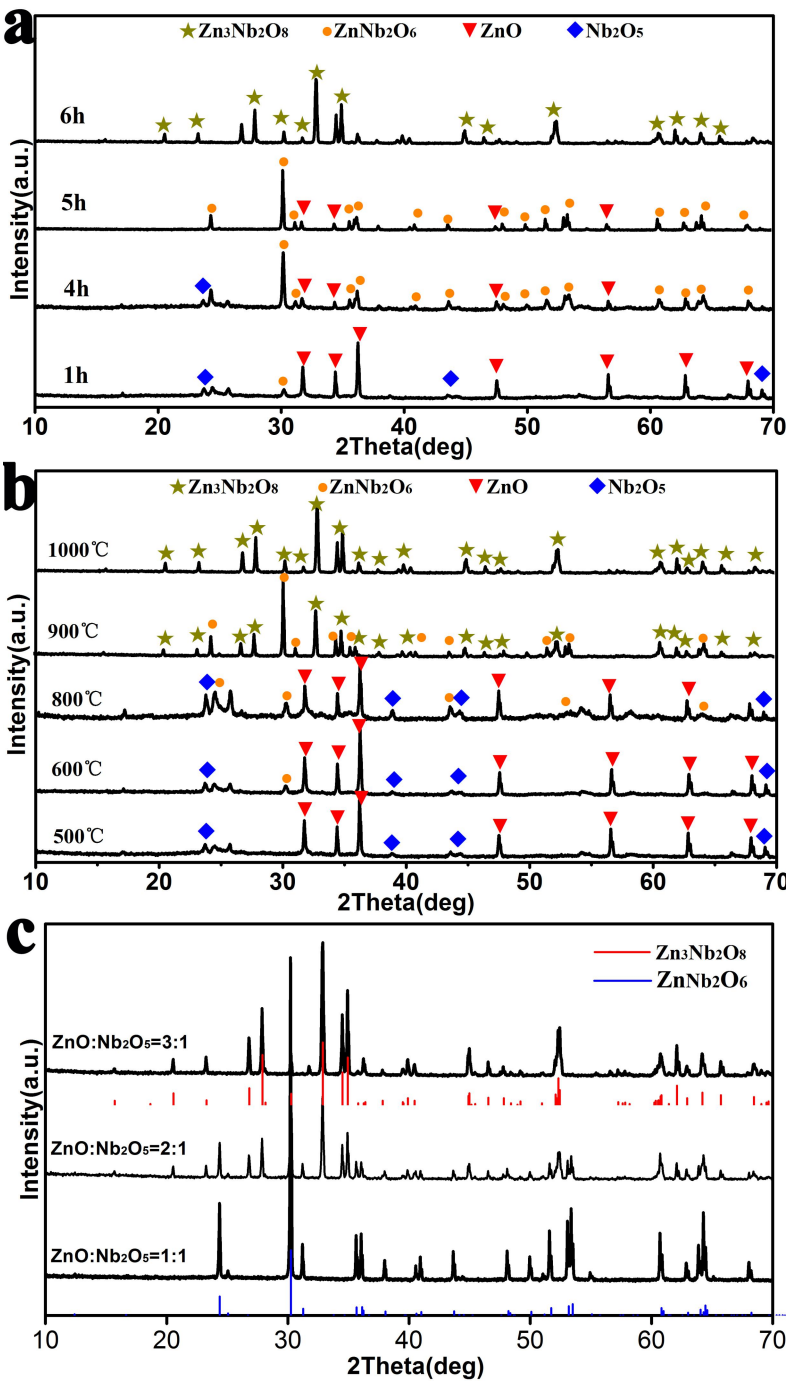

Fig. S2. XRD patterns of as-prepared products in typical synthesis with different duration (a), temperature (b) and the ratio of raw materials (c).

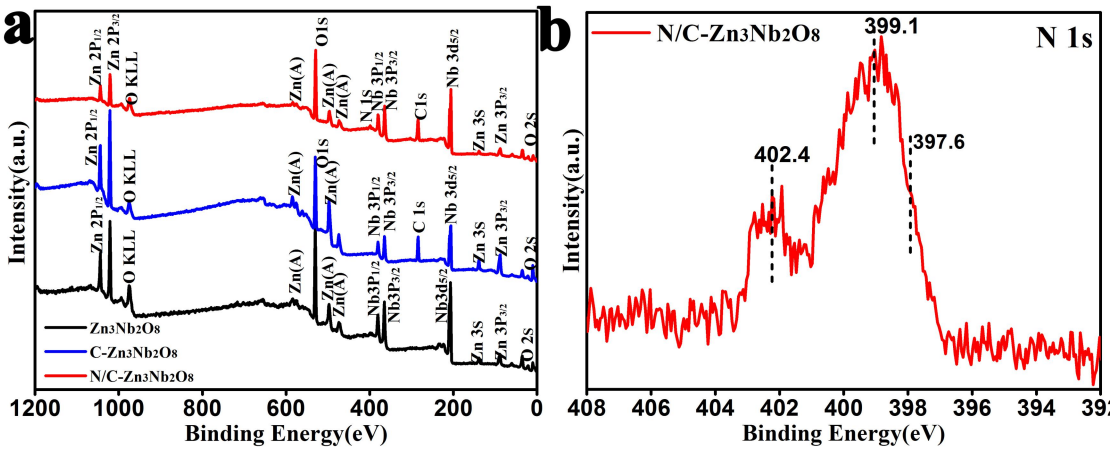

Fig. S3. (a) Full XPS spectrum of the as-prepared photocatalysts. The black, blue and red lines represent bare $Zn_3Nb_2O_8$, carbon doped $Zn_3Nb_2O_6$, and nitrogen (10wt.%) and carbon co-doped $Zn_3Nb_2O_8$, respectively. (b) XPS spectra of N 1s of N/C co-doped $Zn_3Nb_2O_8$.

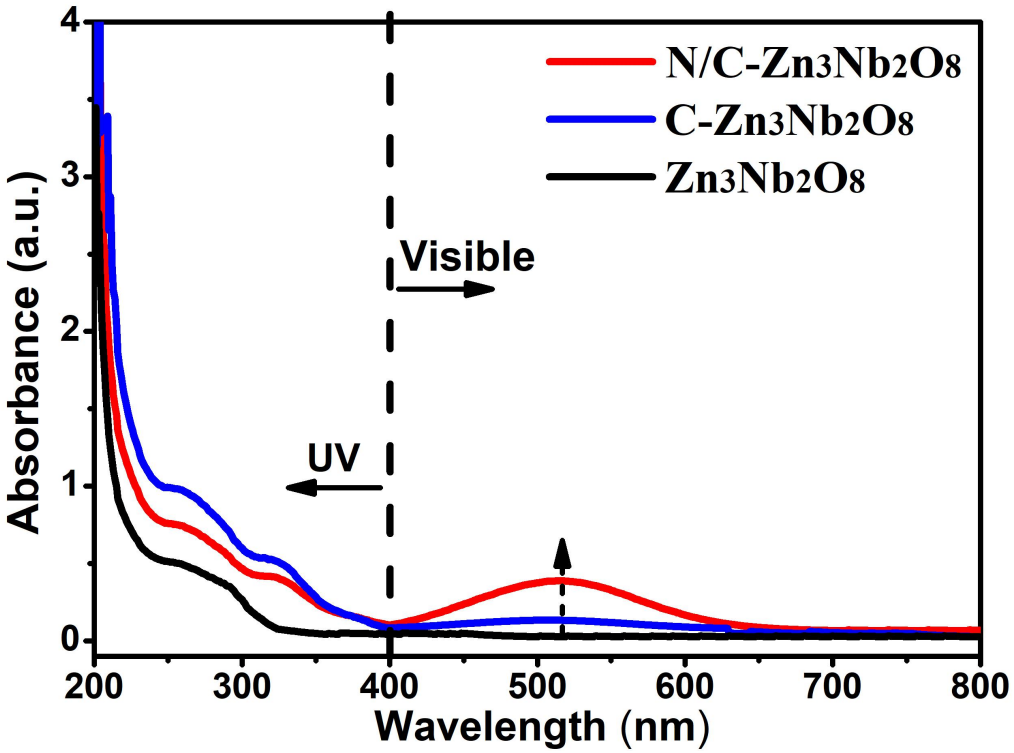

Fig. S4. UV-vis spectrum with the filter of UV elimination ($\lambda \geq 400$ nm) of as-prepared bare $Zn_3Nb_2O_8$, C-$Zn_3Nb_2O_8$ and N/C-$Zn_3Nb_2O_8$ catalysts.

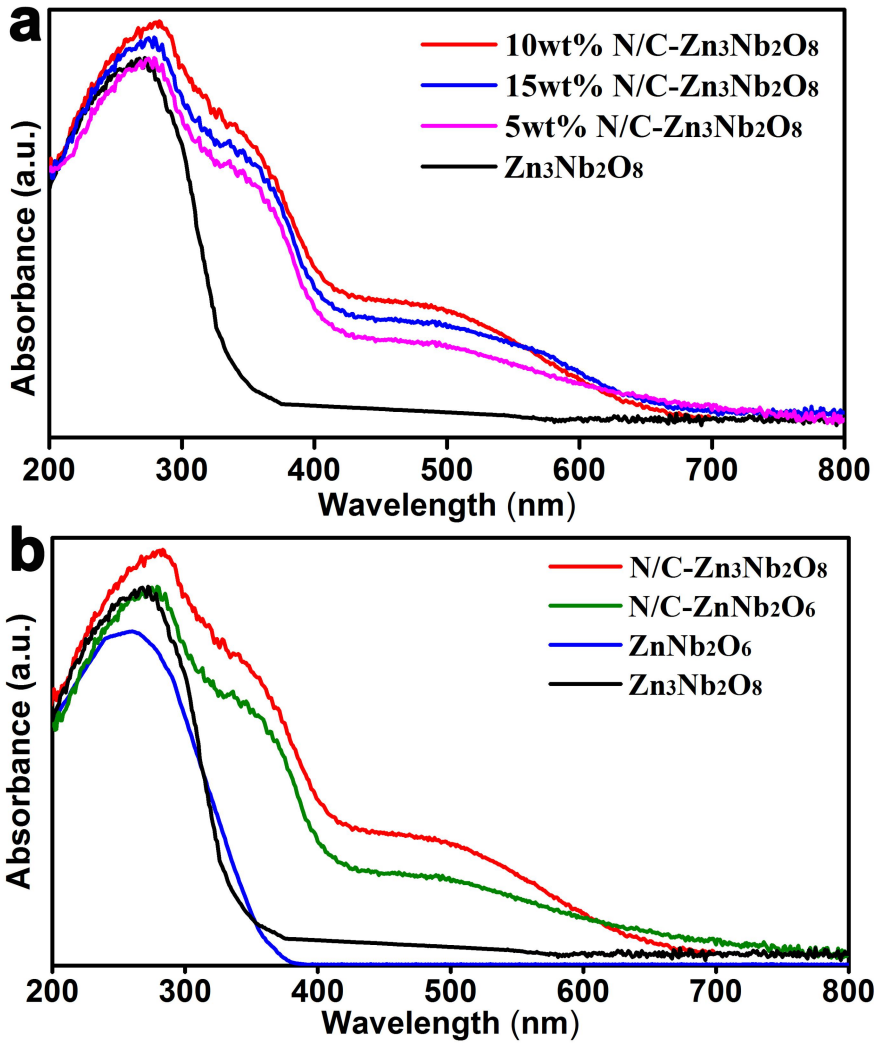

Fig. S5. UV−vis absorption spectra of (a) pure $Zn_3Nb_2O_8$, N/C-doped $Zn_3Nb_2O_8$ with different nitrogen doping concentration, and (b) pure $ZnNb_2O_6$, bare $Zn_3Nb_2O_8$ and their corresponding nitrogen (10 wt.%) and carbon co-doped samples.

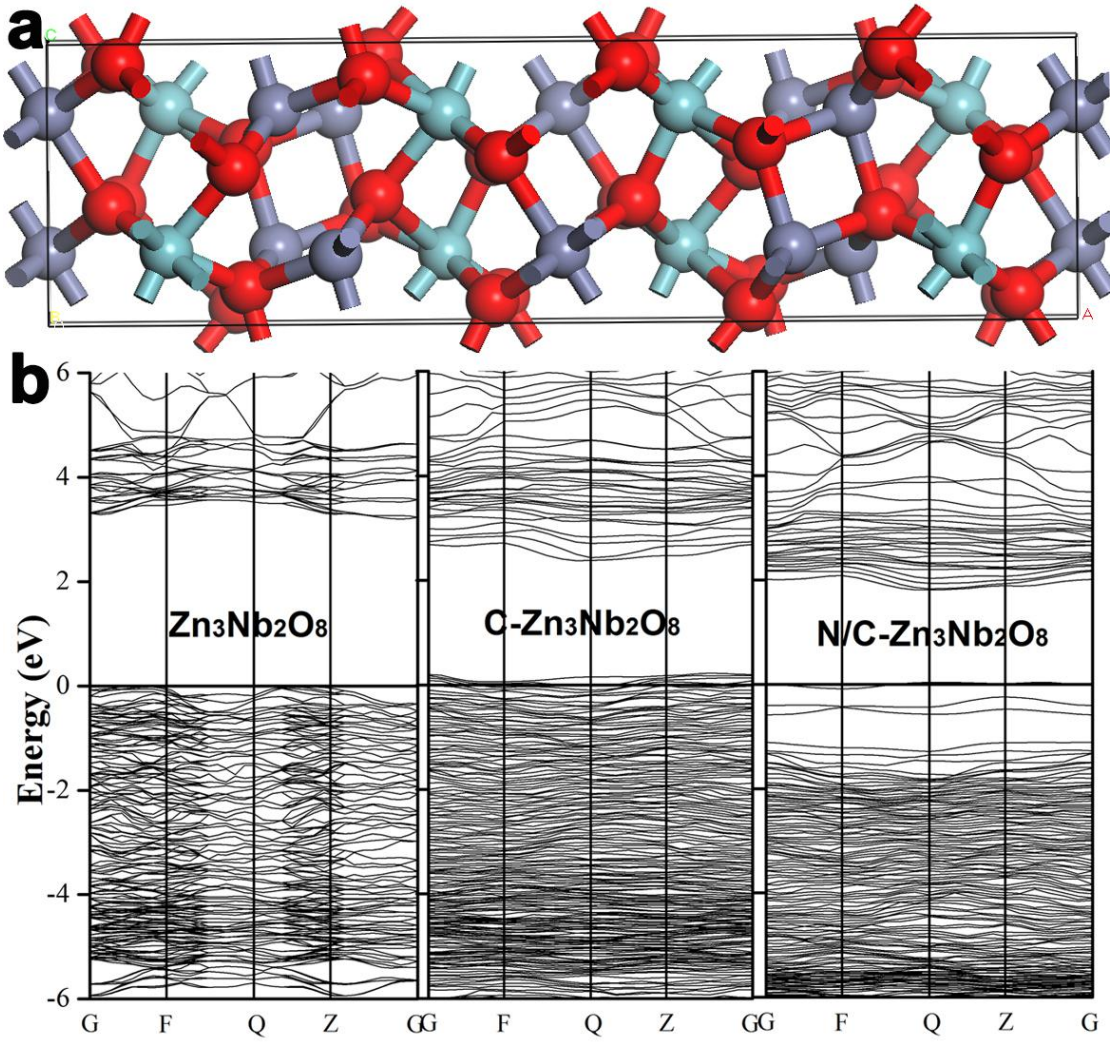

Fig. S6. (a) Lattice structure graph of pure $Zn_3Nb_2O_8$, and (b) band structures of $Zn_3Nb_2O_8$, C doped $Zn_3Nb_2O_8$, C and N co-doped $Zn_3Nb_2O_8$.

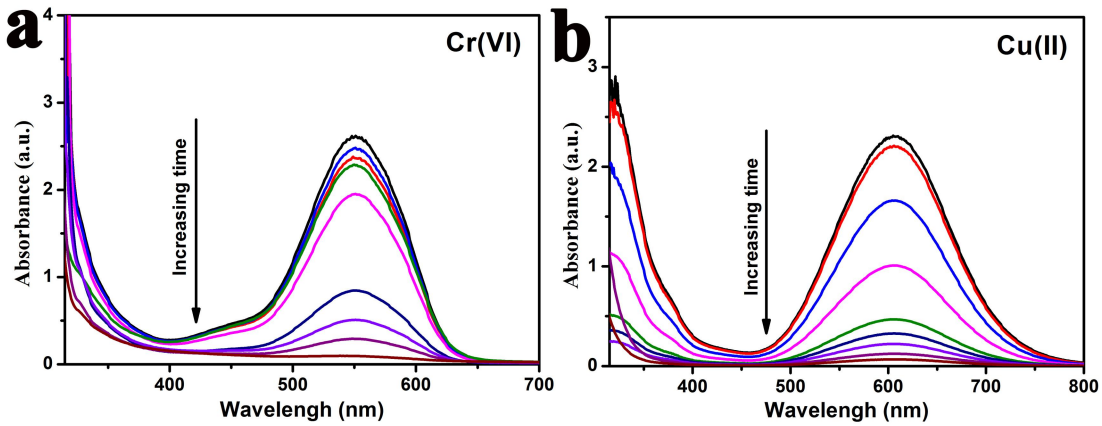

Fig. S7. UV-vis spectral changes of Cr(VI) (a) and Cu(II) (b) in the present of N/C-$Zn_3Nb_2O_8$ catalysts with the increase of visible light irradiation time.

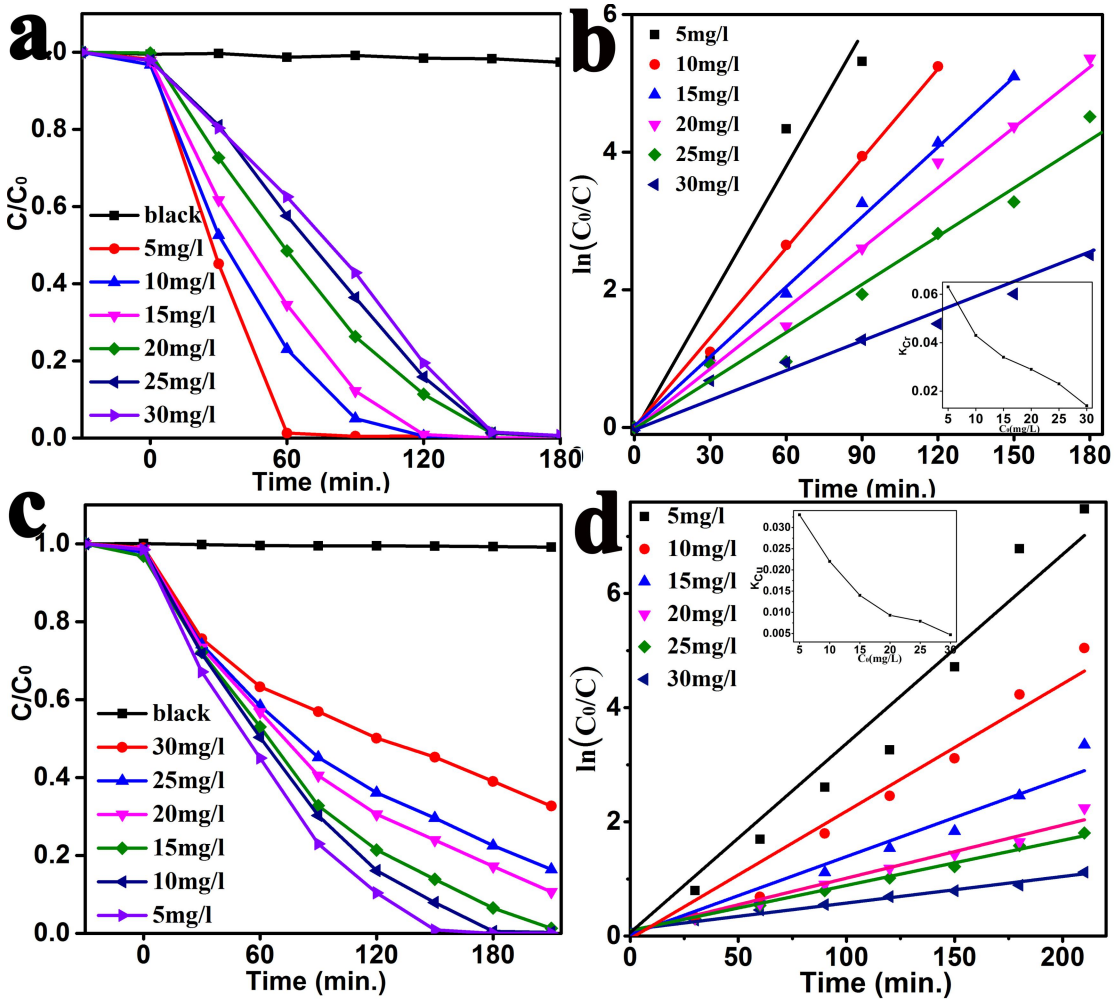

Fig. S8. Reduction efficiency of Cr (VI) (a) and Cu (II) (c), and liner transform $\ln C_0/C$ of the removal of Cr(VI) (b) and Cu (II) (d) over C and N co-doped $Zn_3Nb_2O_8$ catalysts at different initial concentrations. Inset in b and d is the reduction rate at different initial Cr(VI) and Cu (II) concentrations, respectively.

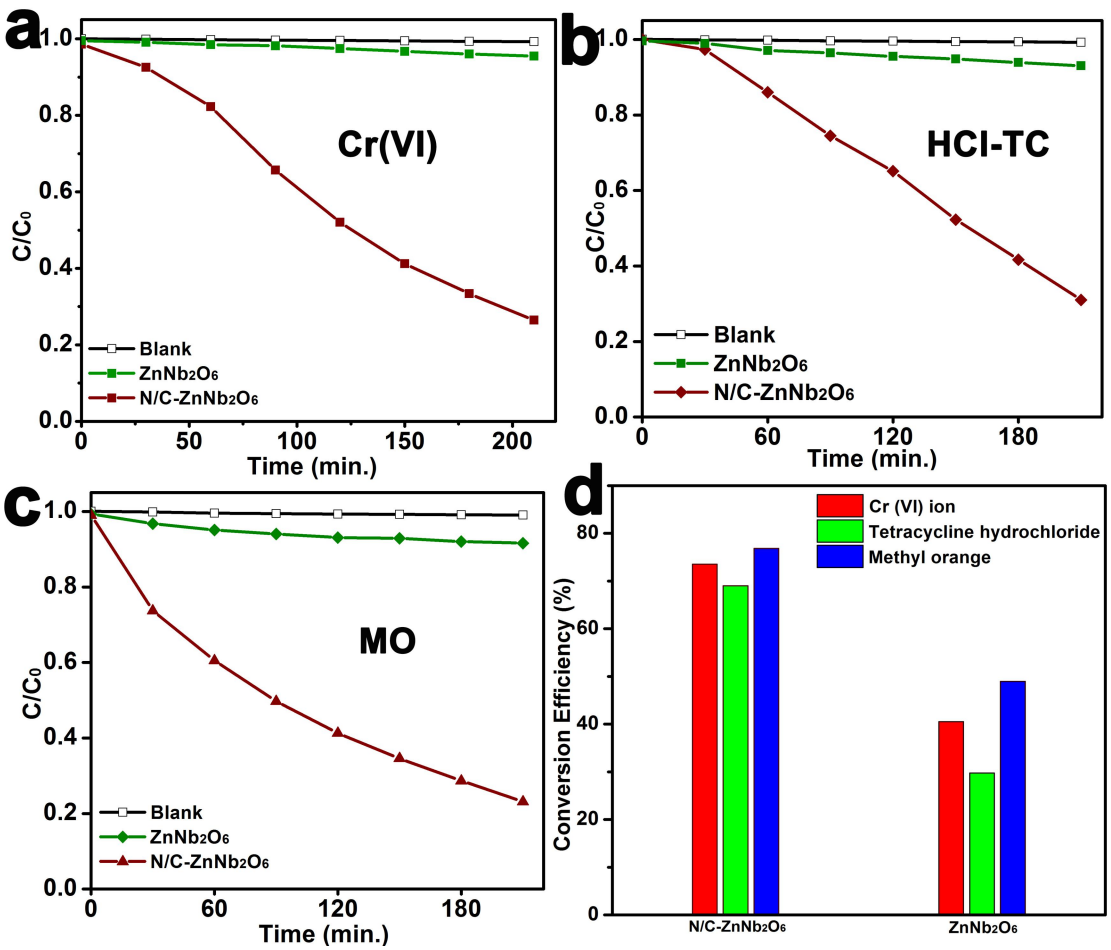

Fig. S9. The concentration changes of Cr (VI) ion (a), tetracycline hydrochloride (b), and methyl orange (c) as a function of visible light irradiation time in the present of pure $ZnNb_2O_6$ and N/C co-doped $ZnNb_2O_6$, and conversion efficiencies in initial 210 min for different photocatalysts (d).

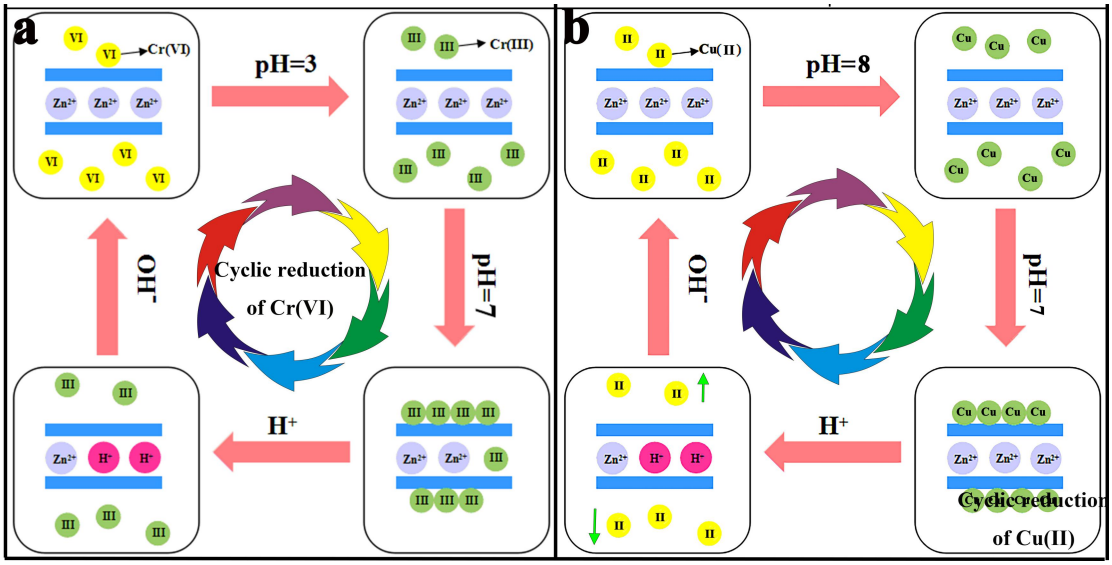

Fig. S10. The schematic diagram for the disposal of chromium species (a) and copper species (b) and the regeneration process of N/C-$Zn_3Nb_2O_8$.